

Number-conserving phase-space dynamics of the Bose-Hubbard dimer beyond the mean-field approximation

F. Trimborn*, D. Witthaut† and H. J. Korsch

Fachbereich Physik, Technische Universität Kaiserslautern, D-67653 Kaiserslautern, Germany

(Dated: February 6, 2020)

The number-conserving quantum phase space description of the Bose Hubbard model is discussed for the illustrative case of two modes and its generalization to an open quantum system. We derive exact evolution equations for the Husimi- (Q) and the Glauber-Sudarshan- (P) -distribution function based on the $SU(2)$ coherent states instead of the usual $U(1)$ -symmetry breaking Glauber states. This description enables us to go even beyond the mean-field limit, since a Liouvillian flow emerges quite naturally in the limit of large particle numbers. Moreover, the deviations from the exact dynamics can be easily estimated. Within the presented approach it is not only possible to take into account arbitrary initial states but also to calculate many quantities, as e.g. variances etc., which are not accessible within the usual mean-field limit. For instance this method resolves the well-known breakdown of the mean-field approximation. A comparison to methods ignoring the fixed particle number shows that in this case artificial number fluctuations lead to ambiguities and large deviations even for quite simple examples. As one possible application of the methods presented here we analyse the time evolution of the coherence between two condensate modes subject to heating caused by collisions with the background gas.

PACS numbers: 03.75.Lm, 03.65.-w

I. INTRODUCTION

The physics of ultracold atoms in optical lattices has made an enormous progress in the last decade, since it is an excellent model system for a variety of fields such as nonlinear dynamics or condensed matter physics. The dynamics of bosonic atoms can be described by the celebrated Bose-Hubbard Hamiltonian, which is a paradigmatic model for the study of strongly correlated many-body quantum systems [1]. Such systems are hard to deal with theoretically since the dimension of the respective Hilbert space increases exponentially both in the particle number and in the number of lattice sites. Therefore, approximations to the dynamics are of considerable interest.

However, things can become surprisingly simple if the atoms undergo Bose-Einstein condensation. In many situations, the mesoscopic dynamics of a Bose-Einstein condensate (BEC) is extremely well described by the (discrete) Gross-Pitaevskii equation (GPE) for the macroscopic wavefunction of the condensate (see, e.g., [2]). This mean-field description is often referred to as 'classical' since the macroscopic limit $N \rightarrow \infty$ of the dynamics in second quantization is formally equivalent to the limit $\hbar \rightarrow 0$ which yields classical mechanics as the limit of single particle quantum mechanics. In practice, this approximation is frequently derived within a Bogoliubov approach, factorizing the expectation values of products of operators into the product of expectation values. As a

consequence there is no obvious indicator to quantify the errors or to specify the scope of validity. Moreover, many interesting observables which involve higher moments of quantum state are not accessible within this approximation.

The phase space formulation of quantum mechanics is nearly as old as the theory itself and has a wide range of applications, especially in quantum optics. Beneath the illustrative insight into the dynamics provided by this formulation, many techniques and methods were developed in this context. However, only a small fraction of the literature is dedicated to systems with intrinsic symmetries like the Bose-Hubbard Hamiltonian. In this case the dynamical group is isomorphic to the special unitary group $SU(M)$, with M being the number of lattice sites, reflecting the conservation of the total particle number. A general algorithm to construct phase space distribution functions for systems whose dynamical group has the structure of an arbitrary Lie group such as $SU(M)$ has been developed only eight years ago [3]. It is based on the concept of generalized coherent states introduced by Gilmore [4] and Perelomov [5]. Starting from these states we have surveyed the mathematical foundations of the number conserving phase space description and derived the exact evolution equations for the Husimi Q -function and the Glauber-Sudarshan P -function of the M -site Bose-Hubbard model in a preceding paper [6]. One important consequence of the use of $SU(M)$ coherent states is the different topology of the phase space, which is now isomorphic to $2M - 2$ dimensional Bloch sphere and therefore compact. Moreover, the phase space description based on $SU(M)$ coherent states allows for a deeper analysis of the many-particle-mean-field correspondence, since these states are of high physical significance. As they are equivalent to the fully condensed

*Present address: Institut für Mathematische Physik, Technische Universität Braunschweig, D-38106 Braunschweig, Germany

†Present address: Niels Bohr Institute, University of Copenhagen, DK-2100 Copenhagen, Denmark

product states, they provide an excellent tool to describe derivations from the macroscopic state.

In this paper we will illustrate the methods originally developed for the M site system [6] for the illustrative case of a two-mode Bose Hubbard model

$$\hat{H} = -\Delta \left(\hat{a}_1^\dagger \hat{a}_2 + \hat{a}_2^\dagger \hat{a}_1 \right) + \epsilon_2 \hat{a}_2^\dagger \hat{a}_2 + \epsilon_1 \hat{a}_1^\dagger \hat{a}_1 + \frac{U}{2} \left(\hat{a}_1^{\dagger 2} \hat{a}_1^2 + \hat{a}_2^{\dagger 2} \hat{a}_2^2 \right), \quad (1)$$

and its generalization which takes into account the coupling to the background gas described by a master equation. Such a two-mode system was realized experimentally by confining a BEC in a double-well trap [7, 8, 9]. Furthermore, this model can describe the fundamental phenomena of two weakly coupled BECs in more general setups [10]. Early theoretical studies of the system dynamics without an external influence were reported in [11, 12].

The paper is organised as follows: First, we briefly recall the main results from the number conserving phase space approach and provide some illustrative examples. Then follows an analysis of the exact dynamics of the quasi probability distributions. Here, we are especially interested in the macroscopic limit, since the evolution equations converge to a classical Liouville equation for large particle numbers. This result enables us to go beyond the usual mean-field limit and to enhance the region of applicability of the approximation. As an example, we show that the Liouville dynamics resolves the so called break-down of the mean-field approximation. A comparison to methods based on a $U(1)$ symmetry breaking description using common Glauber coherent states shows that in this case the deviations from the exact dynamics are significantly larger and appear on a shorter time scale compared to the number conserving approach. The methods developed in [6] are not restricted to the Bose-Hubbard model, but can be applied to every problem with the same symmetry. By the same token, the mapping of operator equations onto partial differential equations for quasi phase space distributions is a general tool for systems whose dynamical group is isomorphic to $SU(2)$. As one possible application, we discuss the heating of a BEC resulting from elastic scattering with the background gas.

II. ALGEBRAIC STRUCTURE AND GENERALIZED COHERENT STATES

The number conserving phase space description of the Bose-Hubbard dynamics has been introduced in [6], starting from the generalized coherent states of Gilmore [4] and Perelomov [5]. Here we will only recall the main results for the special case of two modes for the sake of completeness.

Generalized coherent states for arbitrary dynamical Lie groups are defined by the action of a translation

operator onto a reference state. For instance, the celebrated Glauber coherent states for the Heisenberg-Weyl group H_4 are defined by the relation $|\alpha\rangle = \hat{D}(\alpha)|0\rangle = e^{\alpha \hat{a}^\dagger - \alpha^* \hat{a}}|0\rangle$, where the reference state is just the vacuum state. The parameter space of the translation operators $\hat{D}(\alpha)$ and thus the space of the coherent states is isomorphic to the classical phase space $\mathbb{C} \simeq \mathbb{R} \times \mathbb{R}$.

The situation is different for a BEC in a double well trap since the dynamical group is now $SU(2)$ spanned by the angular momentum operators

$$\begin{aligned} \hat{J}_x &= \frac{1}{2} \left(\hat{a}_1^\dagger \hat{a}_2 + \hat{a}_2^\dagger \hat{a}_1 \right) \\ \hat{J}_y &= \frac{i}{2} \left(\hat{a}_1^\dagger \hat{a}_2 - \hat{a}_2^\dagger \hat{a}_1 \right) \\ \hat{J}_z &= \frac{1}{2} \left(\hat{a}_2^\dagger \hat{a}_2 - \hat{a}_1^\dagger \hat{a}_1 \right). \end{aligned} \quad (2)$$

The Hamiltonian (1) then can be rewritten as

$$\hat{H} = -2\Delta \hat{J}_x + 2\epsilon \hat{J}_z + U \hat{J}_z^2 \quad (3)$$

with $\epsilon = \epsilon_2 - \epsilon_1$ up to a constant term [11, 12, 13]. The Casimir operator $\hat{J}^2 = \hat{N}/2(\hat{N}/2 + 1)$ reveals the relation between the algebraic structure and the total particle number $\hat{N} = \hat{a}_1^\dagger \hat{a}_1 + \hat{a}_2^\dagger \hat{a}_2$.

Generalization of the concept of the translation operator to the $su(2)$ algebra yields an rotation operator, such that the $SU(2)$ or so called Bloch coherent states are defined as follows:

$$\begin{aligned} |\theta, \phi\rangle &= \hat{R}(\theta, \phi)|N, 0\rangle \\ &= e^{-i\theta(\hat{J}_x \sin \phi - \hat{J}_y \cos \phi)}|N, 0\rangle \\ &= \sum_{n_1+n_2=N} \binom{N}{n_2}^{\frac{1}{2}} \cos\left(\frac{\theta}{2}\right)^{n_1} \sin\left(\frac{\theta}{2}\right)^{n_2} e^{-in_2\phi} |n_1, n_2\rangle. \end{aligned} \quad (4)$$

The group of rotations $\hat{R}(\theta, \phi)$ and therefore the parameter space of coherent states can be described by two angles $0 \leq \theta \leq \pi, 0 \leq \phi < 2\pi$ and is thus isomorphic to a Bloch sphere \mathcal{S}^2 . In physical terms, this can be understood as follows: The z -component of the Bloch vector describes the population imbalance of the two modes, while the polar angle represents the relative phase. Since this variable is cyclic and not defined if all particles are in a single well (i.e. at the poles), the topology is clearly that of a sphere.

Instead of a parametrization of the coherent states by the angles θ and ϕ we will frequently use the variables

$$p = \cos^2(\theta/2) \quad \text{and} \quad q = \phi, \quad (5)$$

where p is the population in the second well and q the relative phase of the two modes. Note that the $SU(M)$ coherent states are equivalent to the product states, i.e. they represent a pure condensate. For two modes, $M = 2$, this relation simply reads

$$|\theta, \phi\rangle = \frac{1}{\sqrt{N!}} \left(\cos\left(\frac{\theta}{2}\right) a_1^\dagger + \sin\left(\frac{\theta}{2}\right) e^{-i\phi} a_2^\dagger \right)^N |0, 0\rangle. \quad (6)$$

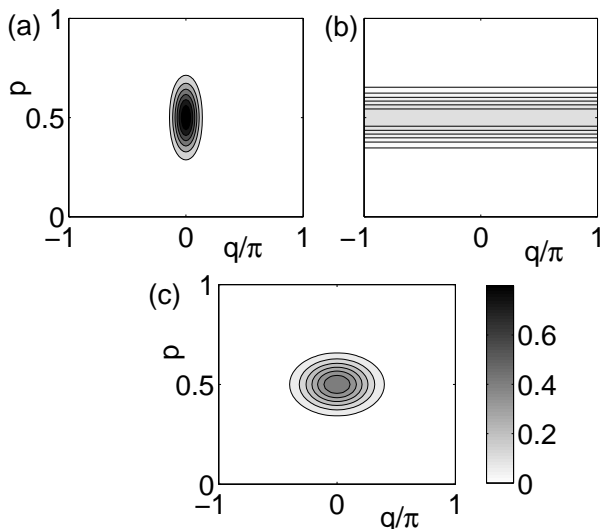


FIG. 1: Husimi functions in a Mercator projection of (a) the coherent state $|p = 1/2, q = 0\rangle$, (b) the Fock state $|n_1 = N/2, n_2 = N/2\rangle$ and (c) the lowest eigenstate of the Hamiltonian (1) for $\Delta = 1$, $U = 10$ and $\epsilon = 0$. The number of particles is $N = 40$ in all plots.

III. PHASE SPACE DISTRIBUTIONS

With the help of the $SU(2)$ coherent states one can readily introduce quasi phase space distributions for a BEC in a double well trap. The Glauber-Sudarshan P -distribution is defined as the diagonal representation of the density operator $\hat{\rho}$ in coherent states

$$\hat{\rho} = \int_{S^2} P(\Omega) |\Omega\rangle \langle \Omega| d\mu(\Omega) \quad (7)$$

where Ω denotes the solid angle and $d\mu(\Omega) = (N + 1)/4\pi d\Omega$ is the invariant measure on the sphere. Due to the overcompleteness of the coherent states, the P -function does always exist but is usually not unique. Furthermore it is not positive definite and often highly singular. On the other hand, the Husimi Q -function defined as the expectation value of the density operator in coherent states,

$$Q(\Omega) = \langle \Omega | \hat{\rho} | \Omega \rangle, \quad (8)$$

is unique, regular and positive definite. Thus the Q -function is especially suited for illustrations, while both quasi distribution functions will be used for actual calculations. However, the Q -function is also not a proper distribution function since it does not give the correct marginal distributions. Note that it is also possible to define the Wigner function on a spherical phase space but this leads to much more complicated expressions than the P - and Q -function, since its construction uses harmonic functions on the respective phase space. This makes actual calculations a hard task even for two lattice sites corresponding to $SU(2)$ (see, e.g., the contradictory re-

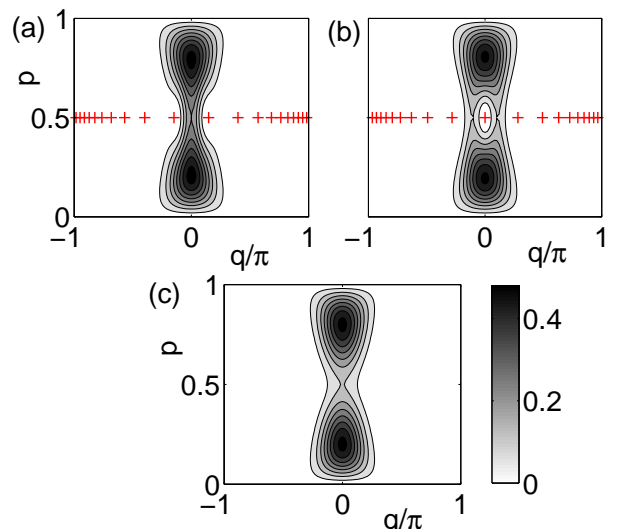


FIG. 2: (Color online) Husimi density of the cat states $|\psi_{\pm}\rangle \propto |0.2, 0\rangle \pm |0.8, 0\rangle$ (a),(b) and the incoherent sum $\hat{\rho}_+ = (|0.2, 0\rangle \langle 0.2, 0| + |0.8, 0\rangle \langle 0.8, 0|)/2$ (c) for $N = 20$ particles. The zeros of the Husimi function are marked by red crosses.

sults in [14] and [15]) and almost impossible for larger systems.

To get a first impression of phase space distributions on the sphere we have plotted the Husimi function for (a) the coherent state $|p = 1/2, q = 0\rangle$, (b) the Fock state $|n_1 = N/2, n_2 = N/2\rangle$ and (c) the lowest eigenstate of the Hamiltonian (1) for $\Delta = 1$ and $U = 10$ in a Mercator projection of the sphere in Fig. 1. The coherent state is maximally localized at the position (p, q) and thus closest to a point in classical phase space. On the contrary a Fock state is localized around $p = n_2/N$. The phase q is completely delocalized in the sense that the Husimi function is uniform in q . Finally one can clearly visualize the number squeezing of the eigenstate (c) in comparison with the coherent state (a) due to the interaction term in the Hamiltonian – a fact which is desirable for matter wave interferometer experiments [16].

The overcompleteness of the basis of (generalized) coherent states guarantees that one can uniquely reconstruct the quantum state out of the quasi probability distribution. It is even possible to determine a pure state solely from the N zeros of the Husimi function or the Bargmann function up to a global phase factor [17]. Thus these zeros carry the essential information about the quantum state and its coherence properties. As an example, Fig. 2 compares the Husimi distribution of a cat state, i.e. a coherent superposition of two coherent states $|\psi_{\pm}\rangle \propto |p = 0.2, q = 0\rangle \pm |p = 0.8, q = 0\rangle$, with the incoherent sum of these two states $\hat{\rho}_+ = (|0.2, 0\rangle \langle 0.2, 0| + |0.8, 0\rangle \langle 0.8, 0|)/2$. The global shape of the Husimi function of the three states appears quite similar with significant differences only around the point $(p, q) = (0.5, 0)$. The Husimi density is increased

for the coherent superpositions $|\psi_+\rangle$ in (a) and decreased for $|\psi_-\rangle$ in (b) in comparison with the incoherent sum, reflecting constructive or destructive interference, respectively. The complete information about the pure states $|\psi_\pm\rangle$ is coded in the distribution of the $N = 20$ zeros of the Husimi function, which are plotted as red crosses in the figure. The Husimi function of the mixed state $\hat{\rho}_+$ has no zero at all, whereas the Husimi function of a coherent state (compare also Fig. 1) has a single N -fold degenerate zero opposite to the maximum of the quasi probability distribution.

IV. DYNAMICS AND THE MACROSCOPIC LIMIT

Evolution equations for the classical phase space distributions can be derived using the mapping of operators in Hilbert space to differential operators on the classical phase space. The \mathcal{D}^ℓ -algebra representation of an arbitrary hermitian operator \hat{A} is defined in a way that both operators have the same effect when acting on a coherent state projector:

$$\hat{A}|\Omega\rangle\langle\Omega| \stackrel{!}{=} \mathcal{D}^\ell(\hat{A})|\Omega\rangle\langle\Omega| \quad (9)$$

$$|\Omega\rangle\langle\Omega|\hat{A} \stackrel{!}{=} \mathcal{D}^\ell(\hat{A})^*|\Omega\rangle\langle\Omega|. \quad (10)$$

The \mathcal{D}^ℓ -algebra representation is well known for the Heisenberg-Weyl algebra. It has been introduced for the $su(M)$ -algebra by Gilmore and coworkers (see [4] and references therein). The evolution equation for the Q -function is then given by

$$\begin{aligned} \frac{\partial}{\partial t}Q(\Omega) &= \text{tr}(\dot{\hat{\rho}}|\Omega\rangle\langle\Omega|) \\ &= -i\text{tr}(\hat{\rho}\hat{H}|\Omega\rangle\langle\Omega| - |\Omega\rangle\langle\Omega|\hat{H}\hat{\rho}) \quad (11) \\ &= -i(\mathcal{D}^\ell(\hat{H}) - \mathcal{D}^\ell(\hat{H})^*)Q(\Omega). \end{aligned}$$

For the P -function we need an associated $\tilde{\mathcal{D}}^\ell$ -algebra defined by an integration by parts:

$$\begin{aligned} \int_{\mathcal{S}^2} \{P(\Omega)\mathcal{D}^\ell(H)\}|\Omega\rangle\langle\Omega|d\mu(\Omega) &= \\ \int_{\mathcal{S}^2} \{\tilde{\mathcal{D}}^\ell(H)P(\Omega)\}|\Omega\rangle\langle\Omega|d\mu(\Omega) \quad (12) \end{aligned}$$

Using this algebra, the evolution equation for the P -function can be derived via

$$\begin{aligned} \dot{\hat{\rho}} &= \int_{\mathcal{S}^2} \frac{\partial}{\partial t}P(\Omega)|\Omega\rangle\langle\Omega|d\mu(\Omega) \quad (13) \\ &= \int_{\mathcal{S}^2} i\left(\tilde{\mathcal{D}}^\ell(H) - \tilde{\mathcal{D}}^\ell(H)^*\right)P(\Omega)|\Omega\rangle\langle\Omega|d\mu(\Omega). \end{aligned}$$

The \mathcal{D}^ℓ -algebra representation of the relevant operators and the evolution equation for the M -site Bose-Hubbard-Hamiltonian have been calculated in the preceding paper [6]. They are generally applicable to every

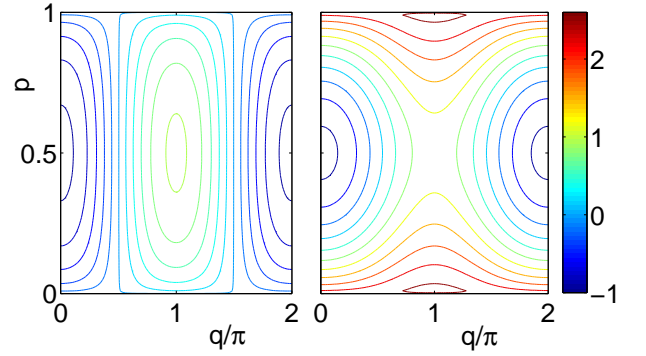


FIG. 3: (Color online) Classical phase space structure: Lines of constant energy $\mathcal{H}(p, q)$ for $J = 1$, $\epsilon = 0$, and $g = 0$ (left) resp. $g = 10$ (right).

problem within this symmetry class. Here, we just quote the exact results for the Q -function in the case of the two sites Bose Hubbard model,

$$\begin{aligned} \frac{\partial}{\partial t}Q(p, q) &= \left\{ +2\epsilon\frac{\partial}{\partial q} \right. \quad (14) \\ &+ \Delta \left(2\sqrt{p-p^2}\sin q\frac{\partial}{\partial p} + \frac{1-2p}{\sqrt{p-p^2}}\cos q\frac{\partial}{\partial q} \right) \\ &\left. + U \left(N(1-2p) - 2p(1-p)\frac{\partial}{\partial p} \right) \frac{\partial}{\partial q} \right\} Q(p, q), \end{aligned}$$

and the Glauber-Sudarshan P -function,

$$\begin{aligned} \frac{\partial}{\partial t}P(p, q) &= \left\{ +2\epsilon\frac{\partial}{\partial q} \right. \quad (15) \\ &+ \Delta \left(2\sqrt{p-p^2}\sin q\frac{\partial}{\partial p} + \frac{1-2p}{\sqrt{p-p^2}}\cos q\frac{\partial}{\partial q} \right) \\ &\left. + U \left((N+2)(1-2p) + 2p(1-p)\frac{\partial}{\partial p} \right) \frac{\partial}{\partial q} \right\} P(p, q). \end{aligned}$$

One can directly show that both evolution equations conserve the normalization. Furthermore it can be shown that the interaction terms $\sim U$ cancel exactly for $N = 1$, since a single Boson obviously does not interact. The expectation values of the angular momentum operators (2) are directly given by the phase space averages [6]

$$\begin{aligned} \langle \hat{J}_k \rangle / N &= (N+2) \int_{\mathcal{S}^2} s_k(p, q)Q(p, q)d\mu(p, q) \quad \text{and} \\ \langle \hat{J}_k \rangle / N &= N \int_{\mathcal{S}^2} s_k(p, q)P(p, q)d\mu(p, q), \quad (16) \end{aligned}$$

where $k = x, y, z$ and

$$\mathbf{s} = \begin{pmatrix} \sqrt{p(1-p)}\cos(q) \\ \sqrt{p(1-p)}\sin(q) \\ p - 1/2 \end{pmatrix} \quad (17)$$

is the classical Bloch vector.

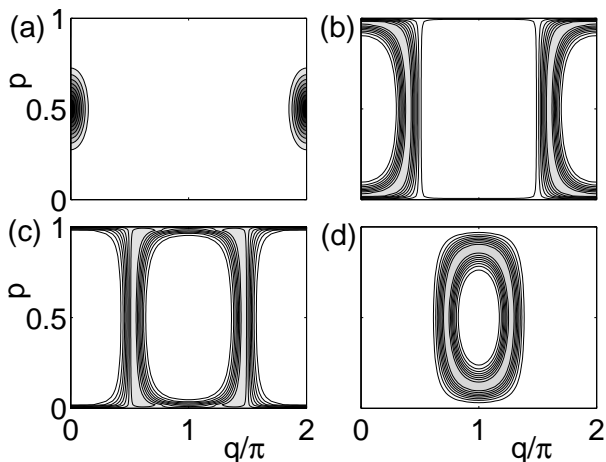


FIG. 4: Husimi density of the eigenstates $|E_n\rangle$ with $n = 1, 15, 23, 34$ (a-d) of the Hamiltonian (1) for $\Delta = 1$, $\epsilon = 0$, $UN = 0$ and $N = 40$ particles. Dark colors encode high values of the Husimi density.

These exact equations provide a valuable starting point to study the limit of large particle numbers, since it emerges quite naturally in the phase space picture. In the macroscopic limit $N \rightarrow \infty$ with $g = UN$ fixed, the second order derivative terms in the evolution equations become negligible, as they are vanishing as $\mathcal{O}(1/N)$. In this case one obtains a Liouville equation for a quasi-classical phase space distribution function $\rho(p, q)$:

$$\begin{aligned} \frac{\partial}{\partial t} \rho(p, q) &= - \left(\frac{\partial \mathcal{H}}{\partial p} \frac{\partial}{\partial q} - \frac{\partial \mathcal{H}}{\partial q} \frac{\partial}{\partial p} \right) \rho(p, q) \\ &= - \{ \mathcal{H}(p, q), \rho(p, q) \} \end{aligned} \quad (18)$$

with the Poisson bracket $\{ \cdot, \cdot \}$ and the Gross-Pitaevskii Hamiltonian function

$$\mathcal{H} = -2\epsilon p - 2\Delta \sqrt{p(1-p)} \cos(q) + \frac{g}{4}(1-2p)^2. \quad (19)$$

The macroscopic interaction strength depends upon the operator ordering and is thus given by $g = UN$ if we start from the Q -function and by $\tilde{g} = U(N+2)$ for the P -function. This difference also vanishes in the macroscopic limit $N \rightarrow \infty$ with $g = UN$ fixed. Therefore the phase space picture gives rise to a Liouvillian flow for the time-evolution of the quasi probability distribution in the macroscopic limit.

The common mean-field limit is subject to even more severe restrictions. To circumstantiate this point, we will have a closer look at the relation between the Liouville dynamics and the GPE. To obtain the latter, one must not only take the macroscopic limit of the evolution equations (14) and (15), but also assume a pure condensate, respectively a $SU(2)$ coherent state which is maximally localized during the whole time evolution. In this case one can approximate the dynamics of a phase space distribution by the dynamics of its center, which is given by

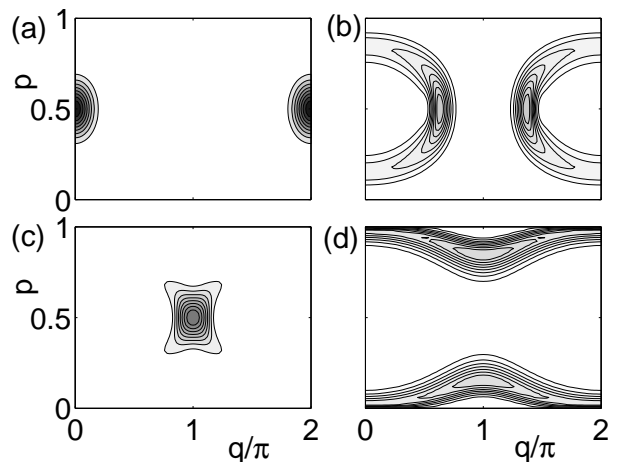


FIG. 5: As Fig. 4, however for $UN = 10$.

the canonical equations of motion

$$\begin{aligned} \dot{p} &= - \frac{\partial \mathcal{H}}{\partial q} = -2\Delta \sqrt{p(1-p)} \sin(q) \\ \dot{q} &= \frac{\partial \mathcal{H}}{\partial p} = -2\epsilon - \Delta \frac{1-2p}{\sqrt{p(1-p)}} \cos(q) - g(1-2p). \end{aligned} \quad (20)$$

These equations are equivalent to the celebrated discrete Gross-Pitaevskii equation

$$i \frac{d}{dt} \begin{pmatrix} \psi_1 \\ \psi_2 \end{pmatrix} = \begin{pmatrix} \epsilon + g|\psi_2|^2 & -J \\ -J & -\epsilon + g|\psi_1|^2 \end{pmatrix} \begin{pmatrix} \psi_1 \\ \psi_2 \end{pmatrix}, \quad (21)$$

if one identifies $\psi_1 = \sqrt{1-p}$ and $\psi_2 = \sqrt{p} \exp(-iq)$ and neglects the global phase. In the non-interacting case $U = 0$, these mean-field equations of motion are exact and an initially coherent state remains coherent in time. However, in the interacting case an initially pure BEC typically deviates quite fast from the set of maximally localized states. Moreover, by approximating the state by a product state one loses the entire information about the higher moments of the state. Therefore many quantities of interest as for example variances etc. are not accessible, whereas they can be easily estimated using the Liouville dynamics and phase space averages similar to (16).

It is important to note that two steps of approximation were necessary to derive the Gross-Pitaevskii equation: In the first step we have neglected the quantum noise term in the evolution equations (14) and (15) which is always possible in the macroscopic limit $N \rightarrow \infty$ with $g \equiv UN$ fixed. Only in the second step to derive the GPE one assumes a nearly pure condensate, so that its phase space representation is strongly localized and can be approximated by a single trajectory in phase space.

Thus it is not only possible to simulate the dynamics of a strongly localized product state, but also of every other possible initial state using the Liouville equation while the error vanishes as $1/N$. Whereas the single-trajectory mean-field approximation will break down if the quantum state differs significantly from a product state, the phase

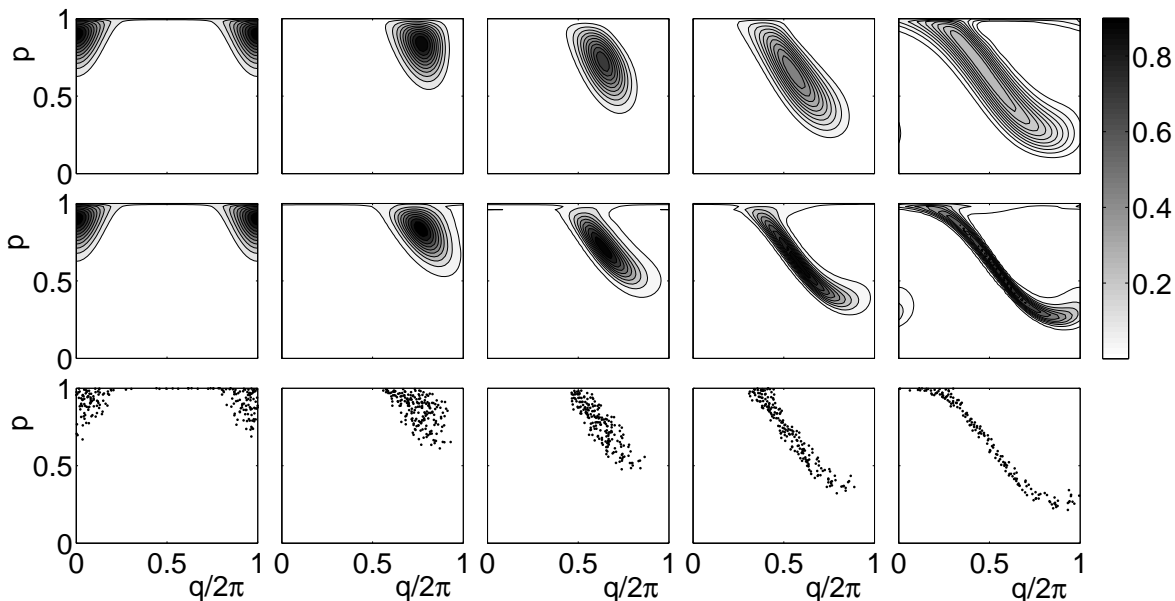


FIG. 6: Breakdown of the mean-field approximation around a hyperbolic fixed point in phase space. Shown is the dynamics of an initially coherent state located at $p_0 = 0.9045$ and $q_0 = 0$ at times $t = 0, 0.12, 0.24, 0.36, 0.48$ (from left to right) for $\Delta = 1$, $UN = 10$ and $N = 20$ particles. The exact quantum evolution of the Husimi function (top) is compared to the classical Liouvillean dynamics (middle) and to the dynamics of a classical phase space ensemble (bottom).

space description still gives excellent results. This issue will be further discussed in Sec. V.

The classical phase space structure induced by the Hamiltonian function (19) is shown in Fig. 3 for $J = 1$, $\epsilon = 0$ and two different value of the interaction strength, $UN = 0$ and $UN = 10$. In the linear case one recovers the simple Rabi or Josephson oscillations. One of the elliptic fixed points bifurcates if the interaction strength exceeds the critical value $UN = 2J$, leading to the self-trapping effect [11, 12].

Furthermore, we have plotted the Husimi function for some selected eigenstates of the Bose-Hubbard Hamiltonian (1) for the linear case $UN = 0$ in Fig. 4 and for $UN = 10$ in Fig. 5. The Husimi functions of the eigenstates localize on the classical phase space trajectories of the respective energy as shown in Fig. 3, where their sum covers the classical phase space uniformly,

$$\sum_n Q_{|n\rangle}(p, q) = 1. \quad (22)$$

In the linear case $UN = 0$, the classical trajectories correspond to the Rabi oscillations between the two wells as shown on the left hand side of Fig. 3. This behavior is directly mirrored by the eigenstates as shown in Fig. 4: The lowest eigenstate localizes on the classical fixed point $(p, q) = (0, 0)$ while the others correspond to Rabi oscillations.

The situation is more interesting, when the interaction strength exceeds the critical value for the self-trapping bifurcation, as shown exemplarily for $UN = 10$ in Fig. 5. For low energies one still finds Rabi modes, while the eigenstates of higher energies correspond to self-trapping

trajectories with a persistent particle number difference and a running phase (cf. Fig. 3, right). However, the eigenstates always localize equally on the trajectories with $p > 1/2$ and $p < 1/2$ because of the symmetry of the Hamiltonian (3). Most interestingly, quantum states can also localize at the unstable hyperbolic fixed point as shown in Fig. 5 (c).

V. RESOLUTION OF THE BREAK-DOWN OF MEAN-FIELD

The phase-space description of the Bose-Hubbard model is especially suited to explore the correspondence of the quasi-classical mean-field approximation and the many-particle quantum dynamics. The established derivations of the Gross-Pitaevskii equation assume a fully coherent quantum state, so that the mean-field approximation is restricted to this class of quantum states. In fact it has been shown that the approximation is no longer valid if the Gross-Pitaevskii dynamics becomes classically unstable [18, 19]. A particular illustrative example of this effect was introduced by Anglin and Vardi [13, 20], who demonstrated the breakdown of the mean-field approximation for a two-mode BEC around the hyperbolic fixed point shown in Fig. 3 on the right-hand side. Therefore, this is an excellent example to demonstrate that the approximation by the Liouville dynamics clearly goes beyond the usual mean-field description and to enlighten the reason of the break-down. The top row of Fig. 6 shows the resulting evolution of the quantum Husimi Q -function. Initially the system is in a fully con-

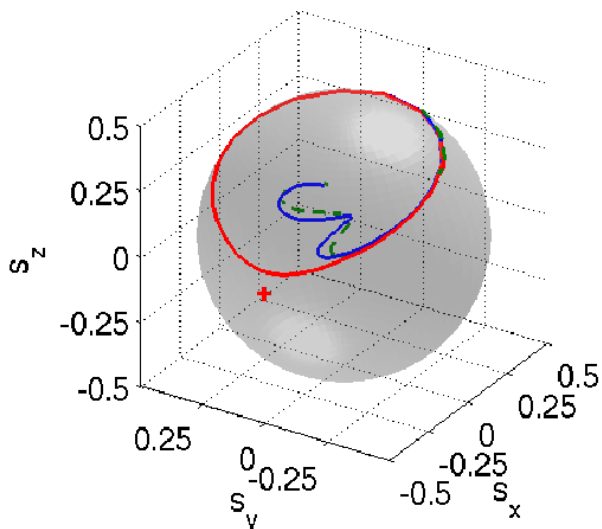


FIG. 7: (Color online) Time evolution of the Bloch vector $\langle \hat{\mathbf{J}} \rangle / N$ approaching the hyperbolic fixed point (solid blue line) for the same parameters as in Fig. 6. The ensemble average over 500 trajectories (dashed green line) closely follows the quantum result, while a single trajectory (solid red line) breaks away in the vicinity of the hyperbolic fixed point (marked by a cross).

densed state, i.e. a $SU(2)$ coherent state at $p_0 = 0.9045$ and $q_0 = 0$, and thus the Husimi function is maximally localized. In the course of time the condensate approaches the hyperbolic fixed point, where the Husimi function rapidly diffuses along the unstable classical manifold. The coherence is lost and the Gross-Pitaevskii equation is no longer valid. This is further illustrated in Fig. 7, where the evolution of the quantum Bloch vector $\langle \hat{\mathbf{J}} \rangle / N$ (solid blue line) is compared to its classical counterpart \mathbf{s} (solid red line). Both agree well in the beginning, when the system is fully condensed. However, the mean-field approximation breaks down as they approach the hyperbolic fixed point (marked by a cross in the figure). The quantum Bloch vector penetrates into the Bloch sphere, while the classical vector \mathbf{s} is restricted to the surface.

However, this breakdown of the mean-field approximation is only due to the neglect of higher moments of the quantum state and not a consequence of a failure of the quasi-classical Gross-Pitaevskii dynamics. Thus it is easily resolved in quantum phase space. The middle row of Fig. 6 shows the evolution of a classical phase space distribution propagated by the Liouville equation (18) which coincides with the Husimi function at $t = 0$. With increasing particle number N the width of the initial distribution decreases such that one recovers a single phase space point in the macroscopic limit $N \rightarrow \infty$. One observes that the classical distribution captures the essential features of the quantum evolution – the spreading along the unstable manifold of the hyperbolic fixed point. Due to the neglect of the second order differential term in Eqn. (14) this spreading is a little overestimated while the

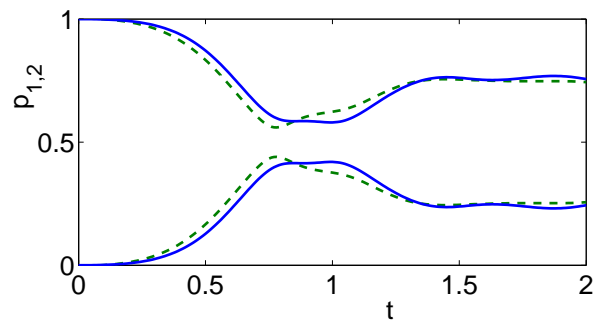


FIG. 8: (Color online) Eigenvalues of the reduced single-particle density matrix (23) calculated from the quantum (solid blue line) and the quasi-classical (dashed green line) Bloch vector depicted in Fig. 7.

quantum spreading in the orthogonal direction is absent. Thus, this can be construed as a disregard of quantum noise which guarantees the uncertainty relation. Furthermore we can interpret the Liouvillian flow in terms of a classical phase space ensemble as shown in the bottom row of Fig. 6. At $t = 0$ this ensemble is generated by 500 phase space points to mimic the quantum Husimi distribution. Afterwards all trajectories evolve according to the Gross-Pitaevskii equation (21) resp. (20). Figure 7 shows the quasi-classical expectation value of the Bloch vector (dashed green line) calculated by the simple phase space average (16) in comparison to the quantum Bloch vector $\langle \hat{\mathbf{J}} \rangle / N$. One observes an excellent agreement. Note that the expectation values calculated from the classical distribution function and the phase space ensemble are indistinguishable on this scale and thus only one curve is shown in the figure.

Finally we want to point out that the phase space picture also provides a quasi-classical description of many-particle quantities that are not accessible within the common single-trajectory mean-field description. In particular one can readily determine the deviation from a pure BEC and calculate the higher moments of the angular momentum operators (2) that can be used to quantify many-particle entanglement [21]. Let us discuss the first issue in more detail. The deviation from a pure BEC can be characterized by the eigenvalues of the reduced single-particle density matrix (SPDM)

$$\rho_{\text{red}} = \frac{1}{N} \begin{pmatrix} \langle \hat{a}_1^\dagger \hat{a}_1 \rangle & \langle \hat{a}_1^\dagger \hat{a}_2 \rangle \\ \langle \hat{a}_2^\dagger \hat{a}_1 \rangle & \langle \hat{a}_2^\dagger \hat{a}_2 \rangle \end{pmatrix}, \quad (23)$$

which are easily found to be given by

$$\lambda_{\pm} = \frac{1}{2} \pm \frac{|\langle \hat{\mathbf{J}} \rangle|}{N}. \quad (24)$$

The leading eigenvalue of the SPDM gives the condensate fraction, i.e. the relative population of the condensate mode [22]. Thus, a BEC is pure if this eigenvalue is equal to one, i.e. if the Bloch vector lies on the surface of the Bloch sphere, $|\langle \hat{\mathbf{J}} \rangle| / N = 1/2$. As discussed

above, the expectation value of the angular momentum operators can be calculated from the quasi-classical phase space distribution function $\rho(p, q)$ in a good approximation. From these it is also possible to reconstruct the SPDM and its eigenvalues completely classically. Furthermore, it is important to note that these quantities are not accessible within a single trajectory mean-field approach, which always assumes a pure BEC. To illustrate this issue we compare the eigenvalues of the SPDM from the quasi-classical Liouville approximation with the exact quantum results in Fig. 8.

Initially one eigenvalue is unity, indicating a pure BEC equivalent to a product state with every particle in the same mode. This eigenvalue decreases rapidly when the Husimi function approaches the hyperbolic fixed point (cf. Fig. 6), indicating a rapid depletion of the condensate mode. One observes that the classical calculation reproduces this depletion of the condensate mode very well.

VI. COMPARISON TO $U(1)$ -SYMMETRY BREAKING METHODS

In the preceding sections we have discussed the number-conserving phase space description of the Bose-Hubbard model avoiding the $U(1)$ symmetry breaking approach, which is however much more common in the literature (see, e.g., for a discussion of dynamics [23] or of ground state properties [24]). The $U(1)$ symmetry breaking phase space description is based on the Glauber coherent states

$$|\alpha_1, \alpha_2\rangle = e^{-(|\alpha_1|^2 + |\alpha_2|^2)/2} \sum_{n_1, n_2=0}^{\infty} \frac{\alpha_1^{n_1} \alpha_2^{n_2}}{\sqrt{n_1! n_2!}} |n_1, n_2\rangle, \quad (25)$$

where the particle number follows a Poissonian distribution. Let us briefly discuss the relation between the phase space representations based on $SU(2)$ and Glauber coherent states.

The Glauber coherent states (25) can be decomposed as

$$|\alpha_1, \alpha_2\rangle = e^{-\frac{\alpha^2}{2}} \sum_{N=0}^{\infty} \frac{\alpha^N e^{-i\chi N}}{\sqrt{N!}} |p, q\rangle_N. \quad (26)$$

into $SU(2)$ coherent states with different particle numbers N , where the respective parameters are related by

$$\alpha_1 = \alpha e^{i\chi} \sqrt{p} \quad \text{and} \quad \alpha_2 = \alpha e^{i\chi} \sqrt{1-p} e^{-iq}. \quad (27)$$

Thus, α is the amplitude and χ is the global phase of the Glauber coherent state. Using this decomposition one can easily relate the Husimi functions based on $SU(2)$ coherent states and Glauber states. Consider an arbitrary many-particle quantum state $\hat{\rho}$ with N particles, which is represented by the $SU(2)$ Husimi function $Q_N(p, q)$.

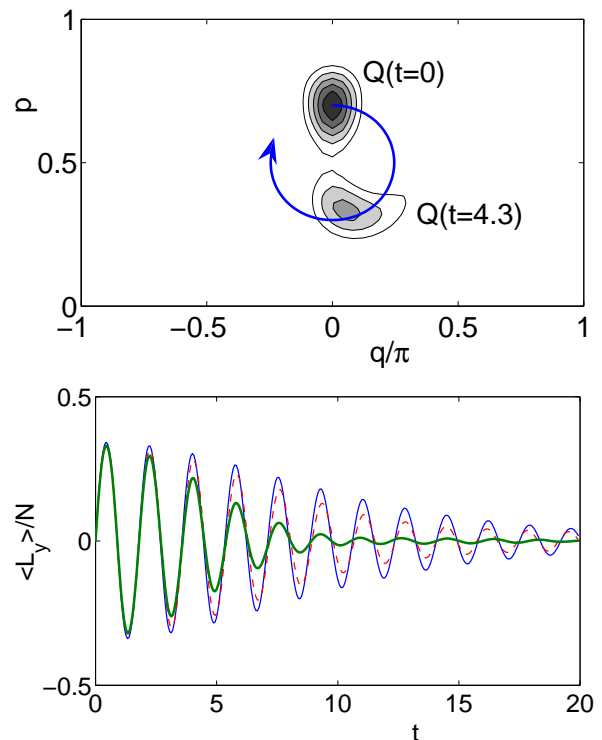


FIG. 9: (Color online) Dephasing of an initially coherent state. Upper panel: Illustration of the dynamics of the $SU(2)$ -Husimi function. Lower panel: Dynamics of the expectation value $\langle \hat{L}_y \rangle / N$ calculated exactly (solid blue line) and quasi-classically from an $SU(2)$ -Husimi distributed phase space ensemble (dashed red line) and a Glauber-Husimi distributed ensemble (thick green line).

The Husimi function in terms of Glauber states is then given by

$$\begin{aligned} Q_{\text{Glauber}}(\alpha_1, \alpha_2) &= \langle \alpha_1, \alpha_2 | \hat{\rho} | \alpha_1, \alpha_2 \rangle \\ &= \frac{e^{-\alpha^2} \alpha^{2N}}{N!} Q_N(p, q) \end{aligned} \quad (28)$$

The physical implications of this mapping are clear: First of all, the Glauber-Husimi representation introduces artificial amplitude noise, since $|\alpha_1|^2 + |\alpha_2|^2 = \alpha^2$ is not fixed but Poisson-distributed. The dynamical effects of this will be discussed below. The classical phase space is then given by \mathbb{C}^2 and the distribution functions thus depend on four variables. In comparison, the approach based on the $SU(2)$ coherent states has some conceptual advantages as it directly embodies the conservation of the particle number N and eliminates the global phase χ . While the particle number is an operator in the $U(1)$ -symmetry breaking approach, it is a parameter in the $SU(2)$ mapping. Thus, the discussion of the macroscopic limit is much simplified, as well as the estimation of the error, which vanishes as $\mathcal{O}(1/N)$. Another approach discussing the convergence to the mean-field approximation by an expansion in terms of the inverse particle number $1/N$ has been reported in [18, 19].

The effects of the artificial amplitude fluctuations can be quite significant. Let us illustrate them with a simple example shown in Fig. 9. We consider the dynamics of an $SU(2)$ coherent state located at $(p, q) = (0.7, 0)$ at $t = 0$ for $J = 1$, $U = 0.1$ and $N = 50$ particles. This state then rotates around the elliptic fixed point of the classical dynamics at $(p, q) = (0.5, 0)$ and so the expectation values of the angular momentum operators (2) oscillate. These oscillations, however, are subject to dephasing and damping because of the quantum fluctuations of the initial state. Fig. 9 shows the dynamics of $s_y = \langle \hat{L}_y \rangle / N$ calculated exactly (solid blue line) and quasi-classically by the propagation of classical phase space ensembles. The ensembles were distributed according to the $SU(2)$ Husimi function (dashed red line) and the Glauber-Husimi function (28) (thick green line). While the damping is well reproduced by the $SU(2)$ ensemble, the artificial amplitude fluctuations of the Glauber-Husimi ensemble cause significant deviations. This is due to the fact that the oscillation frequency around the elliptic fixed point strongly depends on the effective nonlinearity $U\alpha$ and thus trajectories with different normalization α dephase rapidly.

Moreover, already the description of a BEC in terms of $U(1)$ -symmetry breaking states reveals some ambiguities. For instance, consider an $SU(2)$ coherent state, representing a pure BEC. In the framework of the number-conserving phase space description, the P -representation of this state is simply a delta function. On the contrary, the P -function in terms of Glauber coherent states is strongly singular, including high-order derivatives of the delta-function. A pure BEC with a fixed number of particles is thus the most classical state within the $SU(2)$ phase space description whereas it is highly non-classical in terms of the common Glauber phase space picture. In the first case an ensemble representation yields no dephasing at all while such a mapping is simply impossible in the latter case.

VII. HEATING OF A TWO-MODE BEC

Recently, the long-time dynamics of a BEC interacting with the background gas has attracted a lot of interest [9, 25]. It was shown that collisions with the background gas lead to a decrease of the coherence of the two condensate modes, which can be used as a noise thermometer at extremely low temperatures. In this section we want to discuss the heating of a BEC within the quasi-classical phase space picture.

The main source of decoherence and heating is caused by collisions with the background gas atoms and can de-

scribed in leading order by the master equation [26, 27]

$$\begin{aligned} \dot{\hat{\rho}} = & -i[\hat{H}, \hat{\rho}] - \frac{\gamma_1}{2} \sum_{j=1,2} \hat{n}_j^2 \hat{\rho} + \hat{\rho} \hat{n}_j^2 - 2\hat{n}_j \hat{\rho} \hat{n}_j \\ & - \frac{\gamma_2}{2} \sum_{j=1,2} \hat{a}_j \hat{a}_j^\dagger \hat{\rho} + \hat{\rho} \hat{a}_j \hat{a}_j^\dagger - 2\hat{a}_j^\dagger \hat{\rho} \hat{a}_j \\ & - \frac{\gamma_2}{2} \sum_{j=1,2} e^{\beta(\epsilon_j + U\hat{n}_j - \mu)/2} \hat{a}_j^\dagger \hat{a}_j \hat{\rho} + \hat{\rho} \hat{a}_j^\dagger \hat{a}_j - 2\hat{a}_j \hat{\rho} \hat{a}_j^\dagger, \end{aligned} \quad (29)$$

where μ is the chemical potential. The first terms describe elastic scattering events that conserve the number of particles in the condensate mode and only lead to phase decoherence (see, e.g., [28]). Thus they are readily described within the number conserving phase space approach discussed in the present paper, where the interpretation as phase noise becomes especially clear. The second contribution describes inelastic scattering of atoms in and out of the condensate. As argued in [27] this effect is smaller by orders of magnitude for certain trap geometries if the temperatures are low enough and only the ground mode is occupied in every well. Thus we will neglect this amplitude decoherence effect, i.e. we set $\gamma_2 = 0$ in the following.

The effects of the scattering events are conveniently understood and visualized in quantum phase space. The evolution equation for the Husimi function is obtained as in Sec. III by taking the expectation value in $SU(2)$ coherent states:

$$\begin{aligned} \frac{\partial}{\partial t} Q(p, q) &= \langle p, q | \dot{\hat{\rho}} | p, q \rangle \\ &= i \text{tr} \left(\hat{H} \hat{\rho} - \hat{\rho} \hat{H} | p, q \rangle \langle p, q | \right) \\ &\quad - \frac{\gamma_1}{2} \sum_{j=1,2} \text{tr} \left(\hat{n}_j^2 \hat{\rho} + \hat{\rho} \hat{n}_j^2 - 2\hat{n}_j \hat{\rho} n_j | p, q \rangle \langle p, q | \right). \end{aligned} \quad (30)$$

Using the \mathcal{D}^l -algebra representation of the operators introduced above, this equation can be cast into the form

$$\begin{aligned} \frac{\partial}{\partial t} Q(p, q) &= -2 \text{Im}(\mathcal{D}^\ell(\hat{H})) Q(p, q) \\ &\quad - \frac{\gamma_1}{2} \sum_{j=1,2} (\mathcal{D}^\ell(\hat{n}_j) - \mathcal{D}^\ell(\hat{n}_j)^*)^2 Q(p, q) \\ &= -\{\mathcal{H}(p, q), Q(p, q)\} \\ &\quad - 2Up(1-p) \frac{\partial^2}{\partial p \partial q} Q(p, q) + \gamma_1 \frac{\partial^2}{\partial q^2} Q(p, q), \end{aligned} \quad (31)$$

with the classical Hamiltonian function (19). By an analogous calculation one finds the evolution equation for the Glauber-Sudarshan distribution:

$$\begin{aligned} \frac{\partial}{\partial t} P(p, q) &= -\{\mathcal{H}(p, q), P(p, q)\} \\ &\quad + 2Up(1-p) \frac{\partial^2}{\partial p \partial q} P(p, q) + \gamma_1 \frac{\partial^2}{\partial q^2} P(p, q), \end{aligned} \quad (32)$$

keeping in mind that the macroscopic interaction strength is now given by $\tilde{g} = U(N+2)$ instead of $g = UN$.

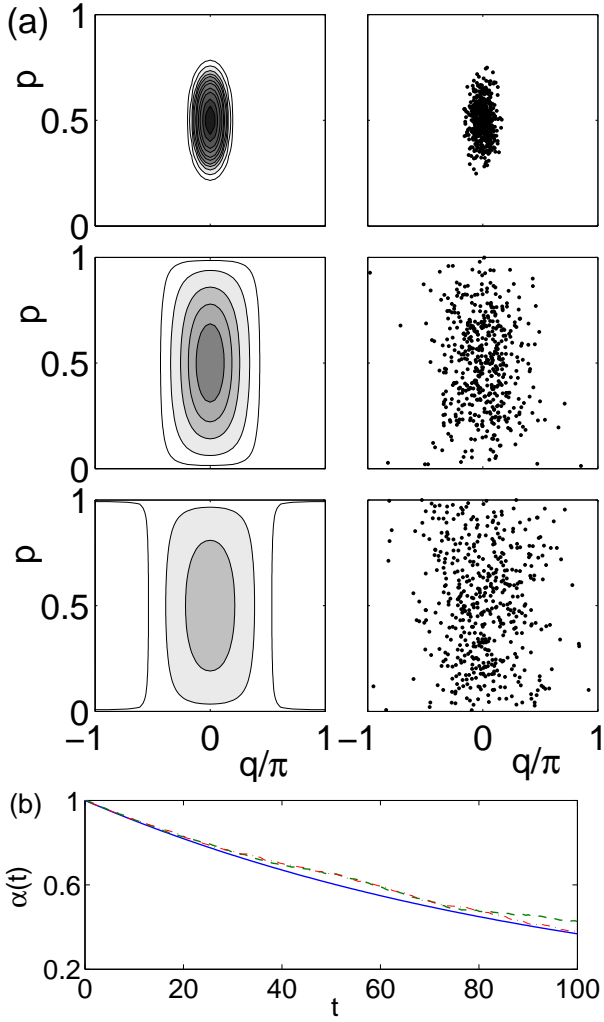


FIG. 10: (Color online) Heating of a two-mode BEC in quantum phase space for $UN = 0$, $J = 1$, $\epsilon = 0$ and $\gamma_1 = 0.01$. (a) Comparison of the exact quantum evolution of the Husimi function $Q(p, q, t)$ (left-hand side) and the stochastic dynamics of a classical phase space ensemble (right-hand side) for $t = 0, 30, 60$ (from bottom to top). Dark colors encode high values of the Husimi density. (b) Decay of the coherence factor $\alpha(t)$. The exact quantum result (solid blue line) is compared to ensemble simulations based on the Q -function (dashed green line) and the P -function (dash-dotted red line).

In these representations the effect of the decoherence term $\sim \gamma_1$ becomes most obvious: It leads to a diffusion of the relative phase of the two condensates and thus to a blurring of the coherence of the two condensates modes. This effect has been directly measured in the experiments of the Oberthaler group [9, 25].

If we neglect the quantum noise term $\sim g/N$, the equations (32) and (33) reduce to Fokker-Planck equations. Thus the condensate dynamics can again be interpreted in terms of phase space ensembles, now subject to the

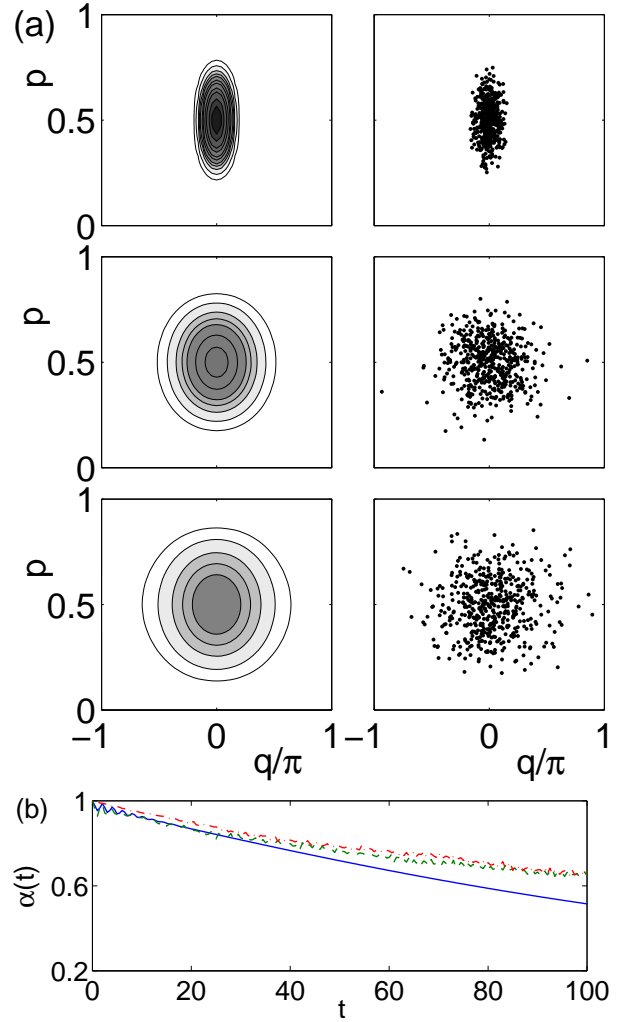


FIG. 11: (Color online) As Fig. 10, however for $UN = 10$.

stochastic evolution equations

$$\dot{p} = -\frac{\partial \mathcal{H}}{\partial q} \quad \text{and} \quad \dot{q} = +\frac{\partial \mathcal{H}}{\partial p} + \sqrt{2\gamma_1} \xi(t), \quad (33)$$

where $\xi(t)$ describes uncorrelated white noise:

$$\langle \xi(t) \rangle = 0 \quad \text{and} \quad \langle \xi(t) \xi(t') \rangle = \delta(t - t'). \quad (34)$$

An example for this quasi-classical description of phase diffusion due to heating of the condensate is shown in Fig. 10(a) for $UN = 0$ and Fig. 11(a) for $UN = 10$, respectively. The left hand side shows the exact quantum evolution of the Husimi distribution $Q(p, q, t)$ calculated from the evolution of the density matrix $\hat{\rho}(t)$ according to the master equation (29). At $t = 0$ the system is assumed to be in a coherent state $|p = 1/2, q = 0\rangle$, i.e., a pure condensate with equal population and zero phase difference between the two wells. In the course of time, the Husimi function spreads and thus the coherence factor $\alpha(t) = \frac{2}{N} \langle \hat{J}_x \rangle_t$ decays as shown in part (b) of the figures. The right-hand sides of Fig. 10(a) and Fig. 11(a) show

the evolution of a classical phase space ensemble initially distributed according to the Husimi function $Q(p, q, 0)$. The single trajectories evolve according to the stochastic equations of motion (33) and thus diffuse over the classical phase space. One observes that the quantum dynamics is well reproduced by the classical approach, especially the different shape of the Husimi function for $U = 0$ and $U = 10$ after the diffusion process.

For a more quantitative analysis we have plotted the coherence factor $\alpha(t)$ in Fig. 10(b) and Fig. 11(b). The quantum result $\frac{2}{N}\langle\hat{J}_x\rangle_t$ is compared to the ensemble averages (16) over 500 classical trajectories for the Q -function and P -function, respectively. In the linear case $UN = 0$ the mapping to stochastic evolution equations is exact and thus the deviations only result from the finite number of classical representations. For $UN = 10$, however, quantum noise is neglected leading to a systematic underestimation of loss of phase coherence.

Furthermore one observes that the coherence factor $\alpha(t)$ decreases much slower for $UN = 10$ compared to the non-interacting case $UN = 0$ both in the exact and in the classical calculation. This difference is readily understood from the structure of the classical phase space as shown in Fig. 3. One observes that the minimum of the classical Hamiltonian function $\mathcal{H}(p, q)$ is much deeper for $UN = 10$, so that the classical trajectories are bound much stronger and phase diffusion is significantly reduced.

VIII. CONCLUSION AND OUTLOOK

In the present paper we have discussed the number-conserving phase space description of the Bose-Hubbard model for illustrative case of two wells and its generalization to an open quantum system. Apart from its theoretic value this system has attracted considerable experimental interest within the last years [7, 9].

We have demonstrated the advantages of the (anti)-normal ordered quasi phase space densities based on the $SU(2)$ coherent states instead of the common Glauber states for the analysis and discussion of quantum states and especially of their dynamics. These representations allow a straightforward comparison of the many-body quantum system and its macroscopic counterpart given by the celebrated Gross-Pitaevskii equation. For instance the quantum eigenstates localize on the classical phase space trajectories. Moreover, we have presented an intuitive way to go beyond the usual mean-field limit: Considering the macroscopic limit $N \rightarrow \infty$ with $g = UN$ without assuming a maximally localized state yields a classical Liouvillian flow for the time evolution of the quasi-probability density or, equivalently, Monte Carlo ensembles of phase space trajectories. In contrast to the usual dynamics described by the GPE, this approach en-

ables us to take into account arbitrary initial states and to estimate quantities depending on higher moments of the quantum state. Obviously this also holds for larger lattices, for which a simulation of the full many-body dynamics is hard.

As an example for the extended scope of application, we consider a BEC approaching a classically unstable fixed point. The condensate fraction rapidly decreases so that the dynamics cannot be described by a single GPE-trajectory any longer. This failure has been denoted as the breakdown of the mean-field approximation in the literature [13, 20]. However, this breakdown is resolved using the Liouville dynamics which provides a quite reasonable approximation for the condensate fraction.

The comparison to methods based on $U(1)$ -symmetry breaking Glauber states shows that even for simple examples the artificial noise in the particle number can result in larger deviations appearing on a much shorter time scale compared to the approach presented here. Moreover, ambiguities in the description of macroscopic states and the set of problems considering the macroscopic limit with \hat{N} being an operator can be tackled easily in the number conserving description where N is simply a parameter. Note, however, that the benefits of a description based on generalized coherent states are not restricted to dynamical problems, see e.g. the semiclassical description of the ground state based on $SU(M)$ coherent states introduced in [29].

The introduction of generalized coherent states and the corresponding phase space distributions opens the door for the use of semiclassical methods for the analysis of the dynamics of the Bose-Hubbard model. The Liouville approach is of course not capable to describe generic quantum effects such as tunneling in quantum phase space and (self-)interference. These features can be reconstructed using semiclassical coherent state propagators (see, e.g. [30, 31] and references therein). In the first part of the present work [6] we have introduced the phase space description and calculated the equations of motion for an arbitrary number of modes. The generalization of the ensemble method to this case is straightforward and allows the approximate calculation of many-particle quantities such as the condensate fraction or higher moments with small numerical efforts. Concrete applications to larger systems will be treated in future research.

Further opportunities include the use of phase space entropies on spherical phase spaces (see, e.g., [17, 32]) to classify quantum states and entanglement.

Acknowledgments

Support from the Studienstiftung des deutschen Volkes and the Deutsche Forschungsgemeinschaft is gratefully acknowledged.

-
- [1] M. P. A. Fisher, P. B. Weichman, G. Grinstein, and D. S. Fisher, *Phys. Rev. B* **40**, 546 (1989).
- [2] L. Pitaevskii and S. Stringari, *Bose-Einstein Condensation* (Oxford University Press, Oxford, 2003).
- [3] C. Brif and A. Mann, *Phys. Rev. A* **59**, 971 (1999).
- [4] W.-M. Zhang, D. H. Feng, and R. Gilmore, *Rev. Mod. Phys.* **62**, 867 (1990).
- [5] A. M. Perelomov, *Generalized Coherent States and Their Applications* (Springer, Berlin Heidelberg New York London Paris Tokyo, 1986).
- [6] F. Trimborn, D. Witthaut, and H. J. Korsch, *Phys. Rev. A* **77**, 043631 (2008).
- [7] M. Albiez, R. Gati, J. Fölling, S. Hunsmann, M. Cristiani, and M. K. Oberthaler, *Phys. Rev. Lett.* **95**, 010402 (2005).
- [8] T. Schumm, S. Hofferberth, L. M. Andersson, S. Wildermuth, S. Groth, I. Bar-Joseph, J. Schmiedmayer, and P. Krüger, *Nature Physics* **1**, 57 (2005).
- [9] R. Gati, B. Hemmerling, J. Fölling, M. Albiez, and M. K. Oberthaler, *Phys. Rev. Lett.* **96**, 130404 (2006).
- [10] C. Orzel, A. K. Tuchman, M. L. Fenselau, M. Yasuda, and M. A. Kasevich, *Science* **291**, 2386 (2001).
- [11] G. J. Milburn, J. Corney, E. M. Wright, and D. F. Walls, *Phys. Rev. A* **55**, 4318 (1997).
- [12] A. Smerzi, S. Fantoni, S. Giovanazzi, and S. R. Shenoy, *Phys. Rev. Lett.* **79**, 4950 (1997).
- [13] A. Vardi and J. R. Anglin, *Phys. Rev. Lett.* **86**, 568 (2001).
- [14] A. B. Klimov, *Journal of Mathematical Physics* **43**, 2202 (2002).
- [15] D. Zueco and I. Calvo, *J. Phys. A* **40**, 4635 (2007).
- [16] G.-B. Jo, Y. Shin, S. Will, T. A. Pasquini, M. Saba, W. Ketterle, D. E. Pritchard, M. Vengalattore, and M. Prentiss, *Phys. Rev. Lett.* **98**, 030407 (2007).
- [17] S. Gnutzmann and K. Zyczkowski, *J. Phys. A* **34**, 10123 (2001).
- [18] Y. Castin and R. Dum, *Phys. Rev. Lett.* **79**, 3553 (1997).
- [19] Y. Castin and R. Dum, *Phys. Rev. A* **57**, 3008 (1998).
- [20] J. R. Anglin and A. Vardi, *Phys. Rev. A* **64**, 013605 (2001).
- [21] A. Sørensen, L.-M. Duan, I. Cirac and P. Zoller, *Nature* **409**, 63 (2003).
- [22] A. J. Leggett, *Rev. Mod. Phys.* **73**, 307 (2001).
- [23] M. J. Steel, M. K. Olsen, L. I. Plimak, P. D. Drummond, S. M. Tan, M. J. Collett, D. F. Walls, and R. Graham, *Phys. Rev. A* **58**, 4824 (1998).
- [24] P. Jain and C. W. Gardiner, *J. Phys. B* **37**, 3649 (2004).
- [25] R. Gati, J. Esteve, B. Hemmerling, T.B. Ottenstein, J. Appmeier, A. Weller, and M. K. Oberthaler, *New J. Phys.* **8**, 189 (2006).
- [26] J. Anglin, *Phys. Rev. Lett.* **79**, 6 (1997).
- [27] J. Ruostekoski and D. F. Walls, *Phys. Rev. A* **58**, R50 (1998).
- [28] D. F. Walls and G. J. Milburn, *Phys. Rev. A* **31**, 2403 (1985).
- [29] P. Buonsante, V. Penna and A. Vezzani, *Phys. Rev. A* **72**, 043620 (2005); P. Buonsante and V. Penna, *J. Phys. A: Math. Theor.* **41**, 175301 (2008).
- [30] M. Stone, K.-S. Park, and A. Garg, *J. Math. Phys.* **41**, 8025 (2000).
- [31] M. Baranger, M. A. M. de Aguiar, F. Keck, H. J. Korsch, and B. Schellhaaß, *J. Phys. A* **34**, 7227 (2001).
- [32] F. Mintert and K. Zyczkowski, *Phys. Rev. A* **69**, 022317 (2004).